EVS30 Symposium
Stuttgart, Germany, October 9 - 11, 2017

On road evaluation of three Hyundai ix35 Fuel Cell Electric Vehicles

P.A. Veenhuizen[1], L.B. Buning[1], M. Merts[1], B. Pyman[1]

[1]*HAN University of Applied Sciences, P.O.Box 2217, NL-6802 CE Arnhem, bram.veenhuizen@han.nl*

Summary

In order to get an improved insight into the capabilities of fuel cell powered vehicles, three Hyundai ix35 vehicles were monitored during 1.5 years and a large number of variables were logged during more than 1500 trips, totalling more than 40.000 km.

This paper presents the data collection procedure, data storage methods and some of the measurement results. Single trip data shows the use of the fuel cell stack and its cooling system. Purging loss for the trip is analysed. Aggregated results for all trips not only cover fuel consumption and electric energy use, but also the internal resistance values for fuel cell stack and high power battery. The fraction of time that the stack is used above a given power level is shown, as well as the average stack power per vehicle. The average electric fuel efficiency for the three vehicles is presented and a comparison is made with state of the art battery electric vehicles. The data presented may be valuable for modelling purposes.

The paper closes by discussing the implications of the findings, drawing some conclusions and presenting an outlook for further work.

Keywords: fuel cell vehicle, hydrogen, energy consumption.

1 Introduction

Hyundai introduced the ix35 FCEV on the European market in 2013 and also in the Netherlands a number of vehicles was leased to various customers, among which the Dutch road authority (2 vehicles) and the municipality of Arnhem (1 vehicle). The HAN University of Applied Sciences was asked to carry out a monitoring study which should give a detailed insight in the technical capabilities of these vehicles. Focus was on fuel consumption, the performance of both the fuel cell stack and the high voltage battery and on a comparison to Electric vehicles and overall vehicle performance. The resulting parameters can be used in vehicle models and simulations.

2 Vehicle description

The Hyundai ix35 Fuel Cell Electric Vehicle (FCEV, see Figure 1) is a compact SUV with specifications, as supplied by Hyundai [1], summarized in Table 1.

Figure 1. Hyundai ix35 FCEV.

Table 1. Vehicle specifications [1].

Vehicle kerb weight	1830 [kg]
Top speed	160 [km/h]
Fuel consumption (NEDC)	0.95 [kg/100km]
PEM Fuel Cell Stack Power (max)	100 [kW], 434 cells
Induction Motor Power, Torque (max):	100 [kW]; 300 [Nm]
Maximum Hydrogen Storage Capacity	5.64 [kg] @ 70 [MPa]
Li-Polymer battery	24 [kW], 0.95 [kWh], nom. 180 [V], 48 cells
Vehicle range (NEDC)	594 [km]

During the test period, three vehicles are monitored simultaneously. Two vehicles are leased by the Dutch road authority and the third by the municipality of Arnhem. The vehicles are monitored in general day-to-day use during more than 1.5 years. The monitoring is still continuing.

3 Data collection and storage

The preparation of the vehicles for automated data collection consisted of two parts, which will be described in the next subsections.

3.1 CAN data preparation

Making use of a Hyundai GDS-M workshop tester, an overview of all available data was made. From this list of over 100 signals a selection was made of signals which were relevant to quantify the behaviour, status and performance of the Fuel tank, Fuel cell system, Driver and the Driveline.

The GDS-M receives data from multiple sources. The GDS-M was used to understand the communication protocol and the format of the data. From this information and using the Vehicle Network Toolbox, a Simulink model was constructed, which could communicate with the GDS-M by simulating vehicle responses. By evaluating the responses of the GDS-M upon sending specific CAN messages, a relation between parameter and CAN-ID could be achieved. By varying the content of each parameter, the applied scaling and numeric format was retrieved. In this way, over 60 signals were identified for storage on a SD card. For example: the signals for the fuel cell system comprised: stack current, stack voltage, minimum and maximum cell voltage and corresponding cell number, in- and outlet air temperature, in- and outlet coolant temperature, coolant pump speed, input coolant pressure, in- and output hydrogen pressure, anode blower speed and airflow.

3.2 Data transmission and storage

For operational convenience, a data acquisition network was devised, which is schematically depicted in Figure 2. The Data Logger labelled IMC BusDAQ in the figure, is connected to a 4g Conel modem. Periodically, after the vehicle is switched off, the data is sent over an OPENVPN connection to an in-company server, and stored in a MySQL database.

In order to reduce file size and 4g communication cost, some slow varying signals (typically temperatures or

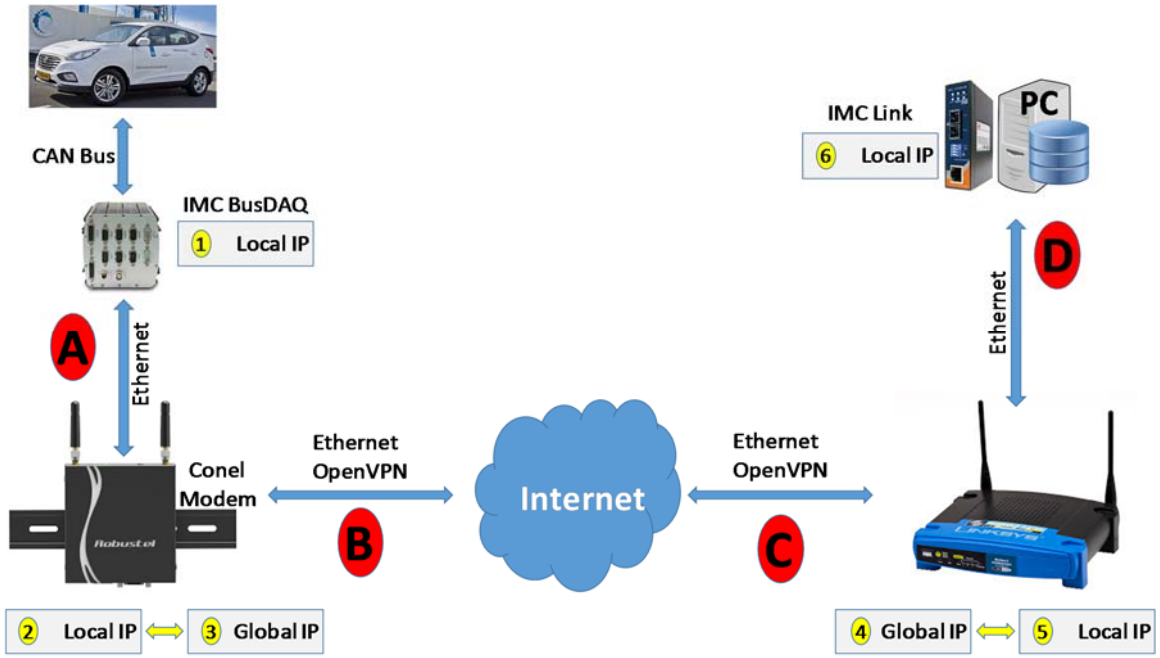

Figure 2. Structure of data acquisition network.

shift lever position) were sampled at a lower rate (0.1 [Hz]) than others (typically voltages and currents, sampled at 5 [Hz]). The procedure allows for completely automated data acquisition, without the need to physically collect the data.

4 Single trip results

Figure 3. Trip indicated by red curve on top of the map of the Netherlands.

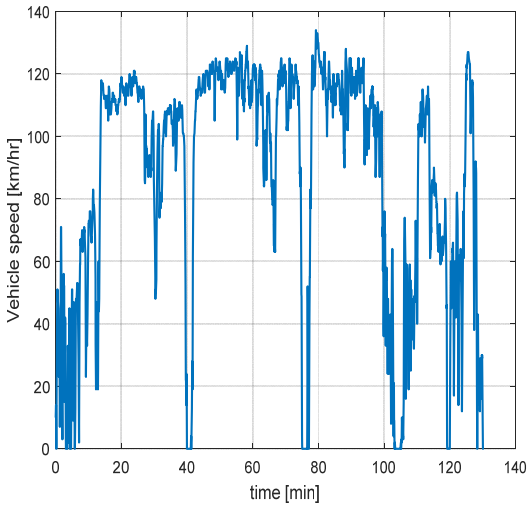

Figure 4. Vehicle speed versus time.

4.1 Trip description

Only one trip (see Figure 3) amongst the more than 1500 measured is selected to present here. The trip was driven by vehicle `iX_35_final_nr1`. It is a rather long trip of 190.1 [km] and 130 [min] starting and ending at the Helmond hydrogen fuelling station. The average speed was 87.5 [km/h]. The speed profile is

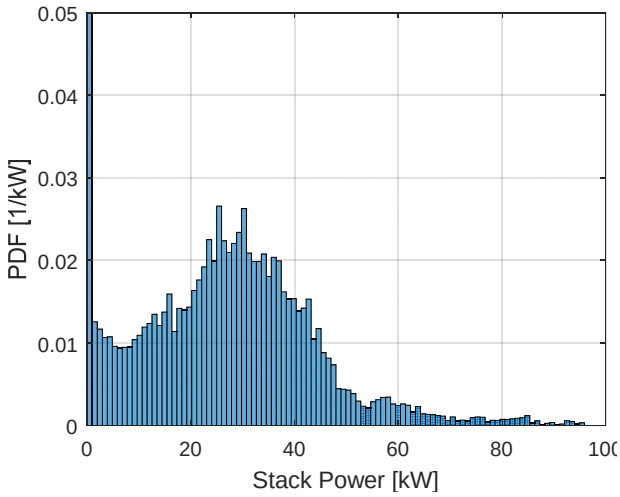

Figure 5. Histogram of fuel cell stack power.

depicted in Figure 4. The fuel cell stack is used at an average power $\frac{1}{T_{trip}}\int_0^{T_{trip}} I_{FC}V_{FC}dt$ = 22.9 [kW], consuming 2.85 [kg] hydrogen. This amounts to a specific fuel consumption of 1.49 [kg/100km].

4.2 Fuel cell stack use

In Figure 5 a histogram of the fuel cell stack power is shown. Typically, the stack is mainly used in part load for all trips.

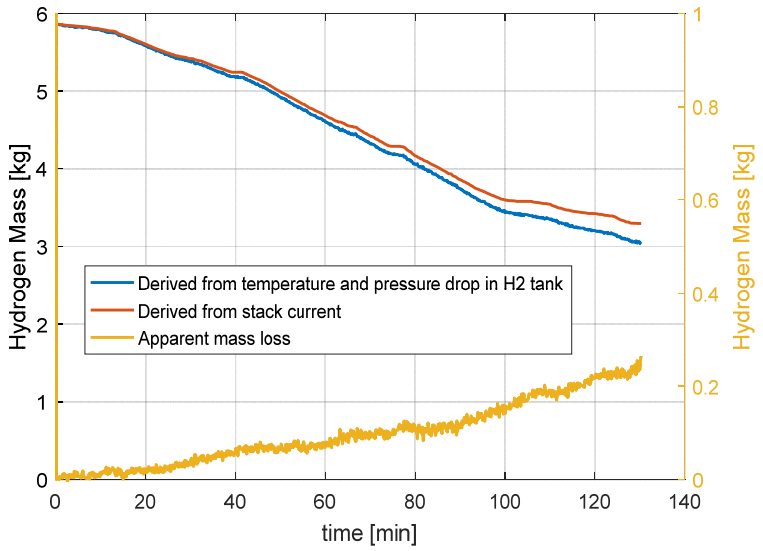

Figure 6. Hydrogen mass versus time. Apparent mass loss represented with respect to scale on the right.

Figure 6 shows (blue line) the reduction of the hydrogen mass $m_{H_2}(t)$ inside the tanks during the trip as derived from both pressure and temperature and using the state equation presented in [2]. Also shown (red line) is the cumulative mass flow as derived from the stack current I_{FC} :

$$\hat{m}_{H_2} = \frac{M_{H_2} N_{cell}}{2F} \int I_{FC} dt + m_{H_2}(t=0), \qquad (1)$$

where M_{H_2} equals the molar mass of hydrogen, $N_{cell} = 434$ the number of cells and F the Faraday constant. The difference between the two lines is also represented in the figure and labelled “Apparent mass loss”. This difference may be attributed to purging or bleeding losses and amounts for this trip to ~0.08 [kg/h].

4.3 Stack cooling system

Figure 7 shows the stack in- and output coolant temperature. The figure shows that the coolant temperature is closely controlled at 60 [°C]. The maximum temperature difference between in- and output for all trips and all three vehicles is found to be 8 [°C].

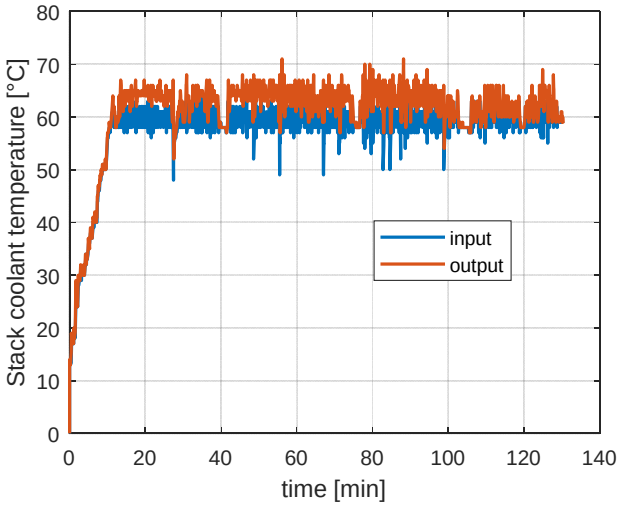

Figure 7. Input and output stack coolant temperature.

5 Aggregated results

This section covers some results per vehicle aggregated over all trips.

5.1 Shift lever and driving modes

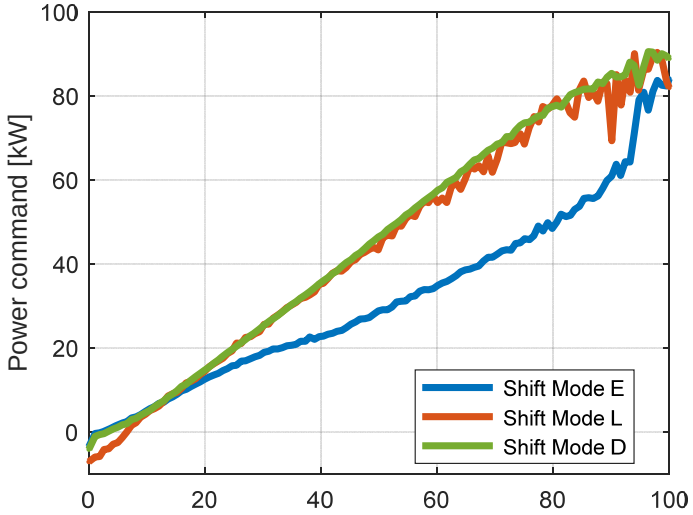

Figure 8. Averaged power command versus relative accelerator pedal position for Economy, Low and Drive shift lever modes.

The power requested from the drive train is shown in Figure 8 for Economy, Low and Drive shift lever settings. This figure is the result of averaging the data for each vehicle. This procedure accounts for the noisy

behavior at higher accelerator values, which occur less frequently than the lower values. The Economy mode is realized by requesting lower power at higher accelerator pedal position (> 20 [%]). At highest accelerator values, the requested power increases in order to allow for maximum power also in E-mode. This behaviour only results in the driver depressing the accelerator pedal deeper in Shift Mode E (compared with Shift Mode D and L), in order to obtain to desired speed. Shift Mode L is equal to Shift Mode D (regular Drive mode), except for low accelerator pedal values, where extra negative power is requested, leading to brake energy regeneration.

5.2 Fuel cell stack use

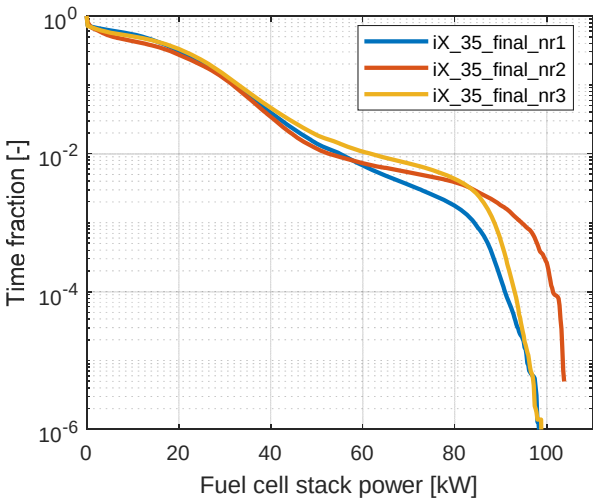

Figure 9. Fuel cell stack use.
For explanation, see text.

Figure 9 shows the fraction of time the fuel cell stack produces power higher than the value on the horizontal axis. For this graph all available data is used, including the time fraction where the stack produces zero power (but contact is switched “on”). For instance, just about 1 [%] of the vehicle operating time the stack produces power higher than ~60 [kW]. See Table 2 for the time that corresponds with 100 [%] for each vehicle. The three vehicles show similar behaviour, but `iX_35_final_nr2` used highest power more than the other two vehicles.

Table 2. Total Contact "on" time for the three vehicles.

Vehicle	**Contact “on” time**
	[h]
iX_35_final_nr1	303.7
iX_35_final_nr2	123.3
iX_35_final_nr3	279.3

5.3 Fuel cell stack air supply

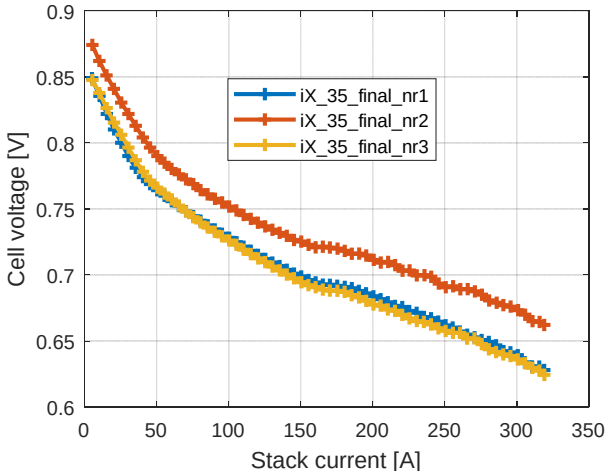

Figure 10. Fuel cell polarization curves averaged over all trips for the three tested vehicles.

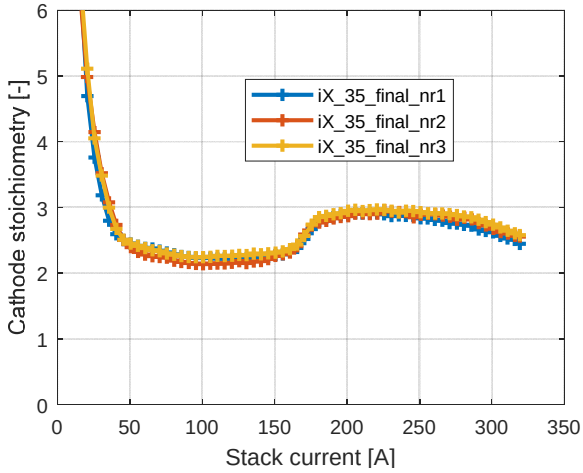

Figure 11. Cathode stoichiometry vs stack current.

By averaging the stack voltage measured at current levels in bins with 5 [A] width, Figure 10 is constructed. In doing this, it is assumed that the voltage response of the stack to a given load current is not disturbed by e.g. temperature or aging. The marked difference between the polarization curve for `iX_35_final_nr2` when compared to vehicle `iX_35_final_nr1` and `iX_35_final_nr3`, cannot be explained yet. All three averaged polarization curves show a minor kink at ~160 [A]. This behaviour can be related to an increase (see Figure 11) in the cathode stoichiometry $\lambda = \left(4Fx_{O_2}\dot{m}_{air}\right)\Big/\left(I_{FC}N_{cell}M_{air}\right)$ for high loads. Here x_{O_2} is the molar oxygen content in air and $\dot{m}_{air}$ and M_{air} represent the air mass flow (measured variable) and the average air molar mass, respectively.

5.4 Battery use

The battery is used for supplying additional driving power and allowing for brake energy recuperation. For the three vehicles the SOC is seen to vary ~35 [%] and ~65 [%] (see Figure 12), but the width at half height of the distribution shown in this figure is just ~15%. This behaviour may be different in mountainous terrain, since more energy can be recuperated driving downhill, possibly leading to higher SOC values.

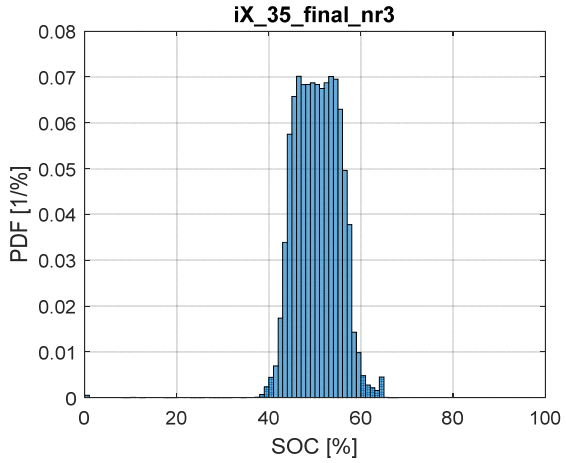

Figure 12. Histogram of the SOC of vehicle `iX_35_final_nr3` for all trips.

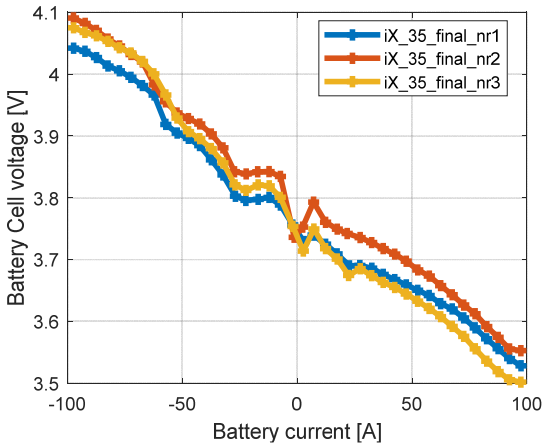

Figure 13. Battery cell voltage vs Battery current, averaged over all trips.

Similar to the procedure mentioned in section 5.3 for the fuel cells, Figure 13 shows voltage versus current for the high voltage battery. Also here, and only roughly, a linear relationship can be seen. The slopes of the lines correspond to effective internal cell resistances, which are multiplied by the number of cells to give the total fuel cell stack or battery internal resistance, as given in Table 3.

5.5 Aggregated electric energy and hydrogen consumption

Figure 14 shows cumulative distance vs cumulative operating time. This means that the time axis only measures the time where the contact is switched on. The figure shows that vehicle `iX_35_final_nr1` has travelled the longest distance at highest average speed, and vehicle `iX_35_final_nr2` travelled only about 6000 [km].

Figure 15 shows the evolution over time for the total energy consumption, which is defined as $E_{total} = \int \left(P_{bat} + P_{FC} \right) dt$, where $P_{bat} = I_{bat} V_{bat}$ and $P_{FC} = I_{FC} V_{FC}$.

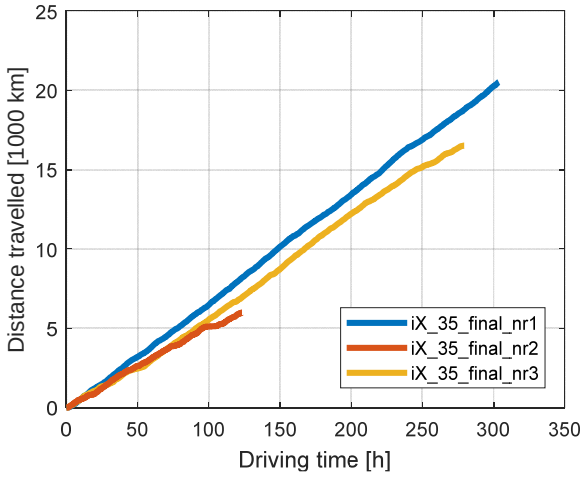

Figure 14. Cumulative distance vs operating time.

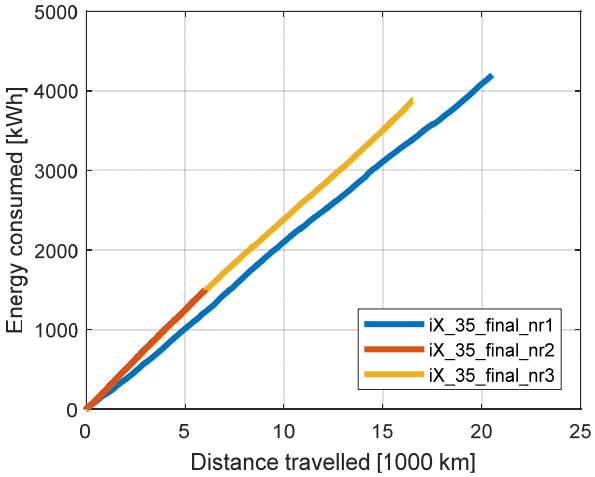

Figure 15. Cumulative energy consumed vs distance travelled.

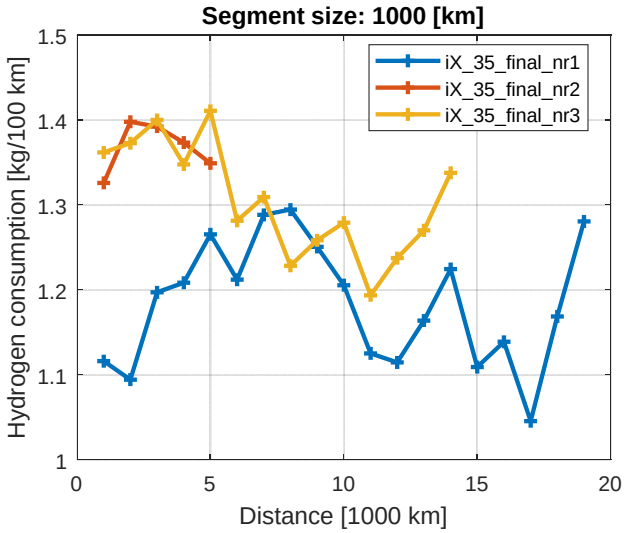

Figure 16. Hydrogen consumed, averaged over 1000 [km] segments.

For Figure 16, the cumulated distance travelled for each vehicle is divided in segments of 1000 [km]. For each segment the fuel consumption per 100 [km] is calculated. The resulting figure shows how the fuel consumption varies due to variations in road load, for instance by wind, temperature, driving style, road condition, etc. The figure shows that real life fuel consumption can be up to 50 [%] higher than the value mentioned by the manufacturer for the consumption on the NEDC (see Table 1).

Table 3 summarizes aggregated data for the three vehicles. Only trips longer than 1 [km] are selected. The table shows that vehicle `iX_35_final_nr1` has a lower average fuel consumption per 100 [km] than the other two. The average purging loss amounts to close to ~0.1 [kg/h] for all three vehicles.

It is interesting to note that although vehicle `iX_35_final_nr1` shows highest purging loss and was driven at highest average speed, it consumes a lower amount of fuel per 100 [km] than the other two vehicles. This is also visible in Figure 16. By selecting only shorter trips for `iX_35_final_nr1`, such that the average trip distance is ~30 [km], the hypothesis was disproven that the relatively low consumption is caused by the longer average trip length for `iX_35_final_nr1.` No other explanation for the difference could be found.

The average stack power is about 15 [kW], which seems remarkably low when a vehicle has 100 [kW] available.

The average electric energy consumption for the three vehicles amounts to 220 [Wh/km] or 350 [Wh/mi]. The average electric fuel efficiency is defined as the ratio of consumed fuel over produced electric energy. The average electric fuel efficiency for the three vehicles, 57.0 [g/kWh], leads to an effective electric energy content of the hydrogen tanks (5.64 [kg]) of 99 [kWh], or 17.6 [kWh/kg], which is 53 [%] of the lower heating value of hydrogen. This number can be regarded as the average stack efficiency for these three vehicles in everyday use. Assuming that the 5.64 [kg] can be used completely, the average fuel consumption per 100 [km] (see Table 3) leads to an average range of 448 [km]. The effective electric energy content of 99 [kW] is close to the energy content of the largest batteries that are in use in present day battery electric vehicles, like the comparable Tesla Model X 100D.

Table 3. Aggregated data for three tested vehicles and trips longer than 1 [km].

Vehicle	**Number of trips**	**Summed distance of all trips**	**Average trip distance**	**Average trip speed**	**Average Fuel cons. per 100 km**	**Average electric efficiency**	**Average hydrogen purging loss rate**	**Average Fuel cell stack power**	**Average Energy consump-tion**	**Average Fuel cell stack internal resis-tance**	**Average Battery internal resis-tance**
	[-]	[km]	[km]	[km/h]	[kg/ 100km]	[g/kWh]	[kg/h]	[kW]	[Wh/km]	[Ω]	[Ω]
iX_35_final_nr1	300	19515	65.0	76.0	1.19	58.3	0.11	14.2	203.5	0.20	0.13
iX_35_final_nr2	170	5416	31.9	66.2	1.37	55.4	0.09	14.5	246.9	0.20	0.12
iX_35_final_nr3	561	14949	26.6	71.0	1.31	56.1	0.08	15.3	233.3	0.22	0.14
All vehicles	**1031**	**39880**	**38.7**	**72.6**	**1.26**	**57.0**	**0.09**	**14.7**	**220.6**	**0.21**	**0.13**

6 Conclusions, outlook

Three Hyundai ix35 Fuel cell vehicles were monitored in considerable detail over a 1.5 year period during everyday use. More than 60 variables were stored during more than 1500 trips, totalling more than 40000 [km]. The data acquisition, transfer and storage system, which was developed largely in house, proved to be very reliable and effective. The vehicles show reliable behaviour, consuming on average 1.26 [kg/100 km], which is ~33 [%] higher than the consumption specified by the manufacturer of 0.95 [kg/100km]. The fuel

cell system is regularly purged, which results in an apparent hydrogen loss rate of ~0.1 [kg/h]. One vehicle (`iX_35_final_nr1`) on average consumed significantly less per distance driven than the other two. No explanation for this phenomenon can be found, so far.

When fully fuelled, the hydrogen tanks have an effective electric energy content of 99 [kWh], which is close to the energy content of the largest batteries in nowadays battery electric vehicles.

Roller test bench data will be reported on in a future paper, as well as results from modelling work that can be used for assessing the performance of the vehicles on alternative driving cycles. Some work is needed on the energy management that is used in the ix35. A next step is the assessment of the sizing of both fuel cell stack and high voltage battery.

Acknowledgements

This work was supported by the Dutch road authority (Rijkswaterstaat) and the municipality of Arnhem. The work was also supported by the RAAK-MKB program of the Nationaal Regieorgaan Praktijkgericht Onderzoek SIA.

References

[1] T. Lim and B. K. Ahn, “Hyundai’s FCEVs: A Pathway to New Possibilities,” *ECS Transactions*, vol. 50, no. 2, pp. 3-10, 2012.

[2] E. W. Lemmon, M. L. Huber and J. W. Leachman, “Revised Standardized Equation for Hydrogen Gas Densities for Fuel Consumption Applications,” *Journal of Research of the National Institute of Standards and Technology*, vol. 113, no. 6, pp. 341-350, 2008.

[3] A. L. W. Vielstich and H. A. Gasteiger, Handbook of Fuel Cells Vol. 1., 1 edition, John Wiley & Sons Ltd, 2003.

[4] National Institute of Standards and Technology, “NIST Fundamental Physical Constants.,” 2014. [Online]. Available: http://physics.nist.gov/cuu/Constants/index.html.

[5] C. d. Cauwer, M. Maarten, S. Heyvaert, T. Coosemans and J. v. Mierlo, “Electric vehicle use and energy consumption based on real world electric vehicle fleet trip and charge data and its impact on existing EV research models,” in *Electric Vehicle Symposium 28*, Goyang, South Korea, 2015.

Authors

Bram Veenhuizen received his masters degree from the Free University in Amsterdam and PhD degree from the University of Amsterdam in 1984 and 1988 respectively.

He joined SKF focussing on electromagnetic and X-ray techniques to characterize materials and material fatigue. In 1995 he joined van Doornes Transmissie (now Bosch Transmission Technology), where he was responsible for the realization of some advanced drive train projects.

In 2002 he was appointed assistant professor at the Eindhoven University of Technology. Since 2005 he is professor in vehicle mechatronics at the HAN University of Applied Sciences.

Lejo Buning received his bachelor's degree in Automotive Engineering in 1984 and his master degree in MBA, in 2014.

He worked on research projects at Technical University of Delft (Transport Systems) National Aerospace Laboratory (Non-Aero and Aerodynamics) and HAN University of Applied Sciences (Automotive Research).

Since 2002 he joined the HAN Automotive Research group as a researcher and project manager on power trains, vehicle dynamics and (after 2015) intelligent mobility.

Menno Merts finished his bachelor automotive engineer at 'HTS Autotechniek' with the development of an alternative-fuel injector in 1998.

He started his career at AG Autogas Systems, where he worked on development of an gaseous fuel system for OEM and aftermarket. In 2004 he joined HAN Automotive as research engineer, working on alternative fuels, engine testing and control, and data-logging.

In 2013 he finished his master in control systems by doing a thesis on engine control by neural networks at FEV.